ELSEVIER

Polymer 42 (2001) 2209–2221

polymer

www.elsevier.nl/locate/polymer

The effect of weld-lines on the morphology and mechanical properties of amorphous polyamide/poly(ethylene-*ran*-propylene) blend with various amounts of an in situ compatibilizer

Jin Kon Kim*, Sang Hyun Park, Hyun Taek O, Hyun Kyung Jeon

Department of Chemical Engineering and Polymer Research Institute, Electronic and Computer Engineering Divisions, Pohang University of Science and Technology, Pohang, Kyungbuk 790-784, South Korea

Received 9 February 2000; received in revised form 29 May 2000; accepted 5 June 2000

Abstract

The effect of weld-lines on the morphology and mechanical properties of 80/20 (wt/wt) amorphous polyamide and poly(ethylene-*ran*-propylene) (EPR) blend with various amounts of maleic anhydride grafted EPR (EPR-M) as an in situ compatibilizer was investigated. In this blend, the effect of crystallization on weld-line strength was completely excluded; thus mechanical properties depend upon the blend morphology and interfacial adhesion strength. As the amount of EPR-M was increased, the dispersed domain sizes were reduced, whereas the shear modulus and the viscosity of the blend increased. We have shown that the injection-molded blend without weld-lines exhibited traditional skin–core morphology. Namely, the dispersed domains at sub-skin layers are strongly elongated toward the flow direction, while those at core regions are not deformed. The sub-skin layer of specimens without weld-lines was significantly reduced with increasing amount of EPR-M. For specimens with weld-lines, the dispersed domains of the blend without EPR-M at sub-skin layer are elongated perpendicularly to the flow direction. However, with increasing EPR-M content, very fine and isotropic morphology is observed.

Both the elongation at the break and Izod impact strength of the weld-specimen increased steadily with increasing amount of EPR-M. But these values are still lower than those of non-weld specimens, even for blends with large amounts of EPR-M. This is because some dispersed domains in weld specimens are elongated perpendicularly to the tensile (or impact) direction. However, the 'V-notch' found at the weld-line of specimens does not affect the mechanical properties. © 2000 Published by Elsevier Science Ltd.

Keywords: Weld-line morphology; Mechanical properties; Reactive polymer blends

1. Introduction

Injection molding is one of the most useful processing methods for obtaining end products made of polymeric resins. But, most injection-molded articles have weld-lines that occur whenever more than two melt fronts meet. Since weld-lines cause reduced mechanical properties and visual defects, many studies have been conducted to explain these weaknesses at the weld-line [1–18]. These weaknesses for homopolymer systems arise from the existence of a 'V-notch', molecular orientations induced by the fountain flow, and poor intermolecular diffusion at the weld-lines. Malaguarnera and Manisali [2] showed that the tensile properties of polypropylene with weld-lines depended very much on the melt and mold temperatures compared with injection speed and pressure.

However, little work [9–18] has been done to investigate the effect of weld-lines on mechanical properties of the polymer blends where the morphology of dispersed domain size and deformation, and interaction parameters between constituent components should be considered. Fellahi and Fisa [10–12] investigated the morphology and tensile strength of weld-line specimens of nylon-6 and high-density polyethylene blend (PA6/HDPE) with a compatibilizer of an ionomer consisting of 80% ethylene and 20% mixture of methacrylic acid with 70% neutralized zinc and isobutyl acrylate. They observed that: (i) the blend with the compatibilizer exhibited reduced thickness of the skin layer, decreased width of the weld-line region and more isotropic weld-line morphology compared with a specimen without the compatibilizer; (ii) tensile strength of the blend increased with the addition of the compatibilizer. Brahimi

* Corresponding author. Tel.: +82-54-279-2276; fax: +82-54-279-8298.
E-mail address: jkkim@postech.ac.kr (J.K. Kim).

0032-3861/01/$ - see front matter © 2000 Published by Elsevier Science Ltd.
PII: S0032-3861(00)00421-3

et al. [13] showed that the mechanical properties of HDPE/polystyrene (PS) blend with a weld-line are much worse than those without a weld-line, and the decrease in properties due to the weld-line is more evident compared with that of the constituent component itself. But, with increasing the amount of a compatibilizer, the mechanical properties of weld-line specimens of the blend sample were much improved. Mekhilef et al. [14] studied weld-line strength of HDPE/polycarbonate blend and the degree of bonding near the interface predicted by a diffusion model with the Flory–Huggins theory was compared with the experimental results. Takeda et al. [15] studied weld-line strength of PA6/poly(2,6 dimethyl-1,4 phenylene ether) (PPE)/PS-*block*-polybutadiene (or poly(ethylene-*co*-butylene))-*block*-PS in the presence of maleic anhydride grafted PPE as compatibilizer. The weld-line strength increased with decreasing weld-line width. Very recently, Jarus et al. [18] studied the weld-line strength of poly(vinly chloride)/HDPE blends. When dispersed domains in a blend are elongated toward the thickness direction of specimens, the blend shows a brittle fracture.

However, to the best of our knowledge, all of the blends investigated in the literature [10–18] contain at least one constituent component that is a semi-crystalline polymer. It is noted that the effect of weld-lines on mechanical properties of polymer is overwhelmed by the crystallization. For instance, tensile properties (such as the elongation at break, ϵ_b) of semi-crystalline polymer (say polypropylene) specimens with weld-line are not reduced much compared to those without weld-lines [3], while ϵ_b of amorphous polymer (say PS or poly(methyl methacrylate) (PMMA)) reduces about one half to one third of that without weld-line [2,4,8].

In order to exclude crystallization effects on the mechanical properties of polymer blend with weld-lines, in this study, we employed an amorphous blend of nylon/poly (ethylene-*ran*-propylene) rubber (AN/EPR). The emphasis was placed on the effect of the amount of maleic anhydride-grafted EPR (EPR-M) as a compatibilizer on the mechanical properties and morphology of the polymer blend without and with the weld-lines. We found that once the dispersed domains are aligned perpendicularly to the tensile direction, the mechanical properties of weld-line specimens are not improved even though the matrix AN chains near the weld-lines could diffuse sufficiently by a long annealing. In this study, we report on the highlights of our findings.

2. Experimental

2.1. Materials

An amorphous nylon (AN) was a commercial grade (SELAR 3426; Dupont Co.) whose chemical structure is given by [19]:

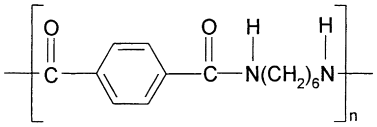

The number-average and weight-average molecular weights (M_n and M_w) were 12,000 and 47,000, respectively [19]. The glass transition temperature (T_g) of the AN was 127°C determined by differential scanning calorimetry (Perkin–Elmer DSC-7 Series) at a heating rate of 10°C/min. An EPR was a commercial grade (KEP020P; KUMHO Polychem Co., Korea). The M_n and M_w were 65,000 and 120,000, respectively. The ethylene content in the EPR was 40 wt% and the T_g of the EPR was −45°C. The compatibilizer employed in this study was an EPR-M (MF-416D; Dupont Co.). According to the producer, the amount of grafted maleic anhydride in EPR-M was 0.5–1.0 wt%. It is well known that the amine group of AN reacts easily with maleic anhydride in the EPR-M to form the graft copolymer having an imide linkage at the AN/EPR interface [20–24].

2.2. Preparation of polymer blend

The AN/EPR blend with various amounts of EPR-M was prepared by using an intermeshing co-rotating twin screw extruder with the barrel length to diameter = 34 and the barrel diameter = 30 mm (TEX 30-30AW-2V, The Japan Steel Works) operating at 255°C and 900 rpm, then pelletized by a rotary cutter. To investigate the effect of the dispersed domain sizes on the mechanical properties, we chose several contents of EPR-M in the blends whose morphologies are pre-determined. For this purpose, the blends were prepared by using an internal mixer (Brabender Co.) with capacity of 30 cc at 255°C and 50 rpm. The blend compositions of AN/EPR/EPR-M employed in this study were 80/20/0, 80/18.8/1.2, 80/16/4, and 80/0/20 (by weight), and referred to as AN–EPR-M(x) where x is the weight percent of EPR-M in total rubber phase (EPR + EPR-M).

2.3. Rheological measurement

To investigate the effect of the amount of EPR-M in the blend, thus the extent of the reaction and the morphology, on the rheological properties, we used an ARES (Rheometrics Co.) using the dynamic oscillatory mode with parallel plate fixture of 25 mm diameter to measure the storage modulus (G'), loss modulus (G''), and complex viscosities ($\eta^*(\omega)$) at wide ranges of frequencies ($0.1 \leq \omega \leq 100$ rad/s).

2.4. Injection molding

All blends were dried at 80°C over 24 h prior to the injection and shaped by using an injection molding machine (IDE140ENII: LG Co. Korea) with a clamping force of 140 t and an injection pressure of 600 MPa. The injection and mold temperatures were 255 and 50°C, respectively. A

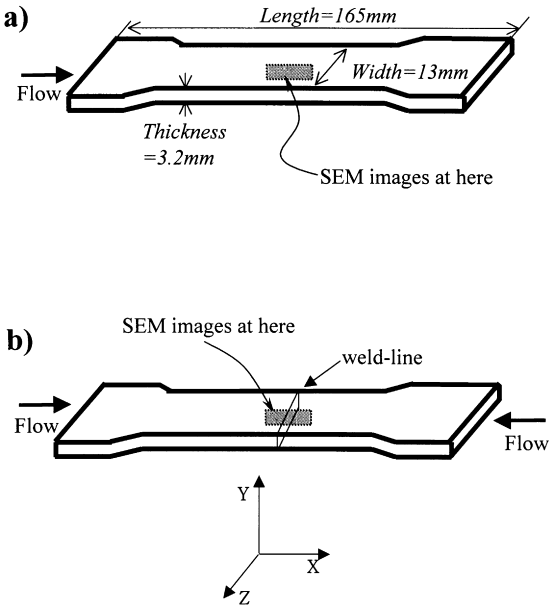

Fig. 1. Schematic of the mold cavity where molten polymers enter the cavity through a film gate: (a) mold dimension without weld-line; and (b) mold dimension with weld-line.

dog-bone shaped molder was used according to the ASTM D638 ($L \times T \times W = 115 \times 3.2 \times 13$ mm^3). The specimen without weld-lines was prepared by using a single-gated molder, as shown in Fig. 1(a). On the other hand, to provide a weld line (cold weld type) in the specimen, a double-gated molder was used as shown in Fig. 1(b). The tensile properties of injection-molded specimens with various content of the EPR-M were obtained by using a universal tensile machine (Instron 4206) with a crosshead speed of 5 mm/min at room temperature.

The specimen for impact properties was prepared according to ASTM D256 ($L \times T \times W = 62.3 \times 3.2 \times 13$ mm^3) by using the same injection molding machine employed in the tensile specimen. Then, we made a notch in the specimens by using a notching cutter (TMI 22-01: Testing Machines Inc.). The specimens with weld-lines were carefully notched at the position where the weld-line was observed. Izod impact strength (IS) was measured with an impact tester (TMI 43-1: Testing Machines Inc.) at room temperature.

2.5. Morphological measurement

A Field Emission Scanning Electron Microscope (S-4200: Hitachi) was used to investigate the morphology of the blends after the specimens at the half width ($z = W/2$) were carefully cut at liquid nitrogen atmosphere. The perpendicular sections to the flow direction (the hatched area in Fig. 1) were observed, namely, the area (xy-plane) containing near half of the length ($x \sim L/2$) and entire thickness. Thus, these images for a weld-line specimen have the weld-line morphology. In order to improve the phase contrast between two phases, the rubber phase in the

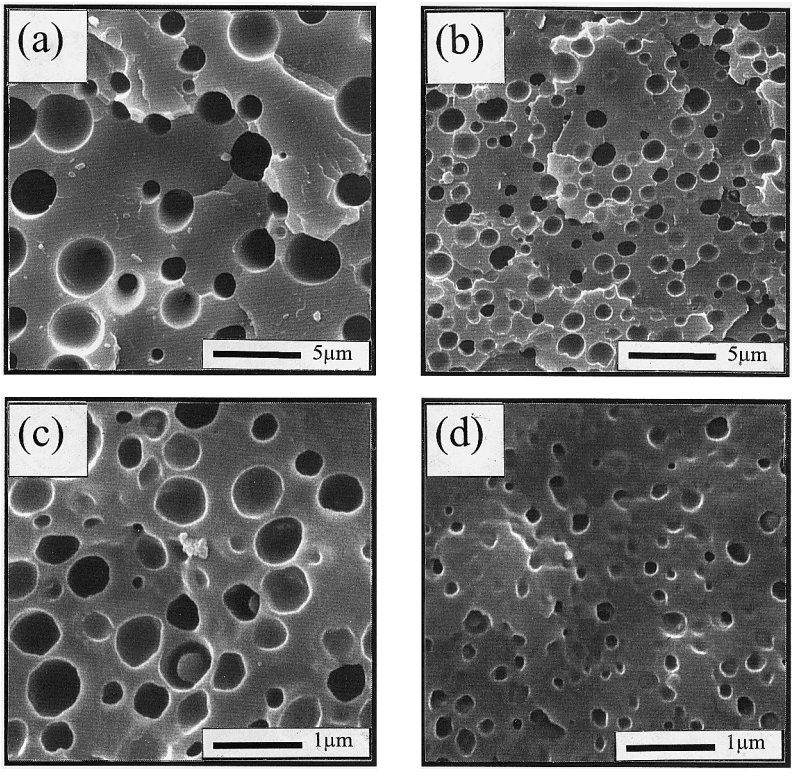

Fig. 2. SEM images of pellet samples prepared by an extruder for all blends: (a) AN–EPR-M(0); (b) AN–EPR-M(6); (c) AN–EPR-M(20); and (d) AN–EPR-M(100).

Table 1
The values of D_n and D_s at core region and L/D of the dispersed phase at skin and sub-skin layer for blends without weld-lines; the values of D_n and D_s for extrudate pellet are also added

		AN–EPR-M(0)	AN–EPR-M(6)	AN–EPR-M(20)	AN–EPR-M(100)
Skin	L/D	6.3	4.9	3.6	2.9
Sub-skin	L/D	6.9	5.5	4.1	2.9
Core	D_n (μm)	1.87	0.75	0.29	0.12
	D_s (μm)	4.5	1.31	0.54	0.18
Extrudate	D_n (μm)	1.9	0.81	0.30	0.11
Pellet	D_s (μm)	2.9	1.0	0.45	0.17

specimen was etched out by toluene for 12 h at room temperature, and coated with a thin layer of gold. The number average (D_n) and the surface area-average diameter (D_s) domain sizes were obtained with a Quantimet 570 image analyzer (Cambridge Instruments) by using at least 200 domains. The cross-sectional area (A_i) of each particle on the SEM micrograph was measured and then converted into the diameter (D_i) of a circle having the same cross-sectional area:

$$D_i = 2(A_i/\pi)^{1/2} \tag{1}$$

Then, D_n and D_s are obtained by

$$D_n = \sum_i D_i/N \tag{2a}$$

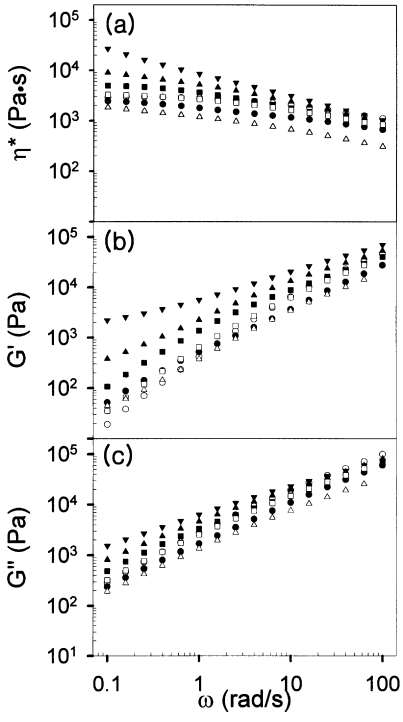

Fig. 3. Plots of (a) η^*; (b) G'; and (c) G'' versus frequency (ω) for various blends as well as neat polymers: (●) AN–EPR-M(0); (■)AN–EPR-M(6); (▲) AN–EPR-M(20); (▼)AN–EPR-M(100); (○) neat AN; (□) neat EPR; (△) neat EPR-M.

$$D_s = \sum_i D_i^3 / \sum_i D_i^2 \tag{2b}$$

where N is the total number of dispersed domains seen in the SEM image.

3. Results and discussion

3.1. Blend morphology and rheology

Fig. 2 gives SEM images of extrudated pellets of AN–EPR-M(x) prepared by a twin-screw extruder. The change in the D_n and D_s with increasing EPR-M is summarized in Table 1. The D_n decreased from 1.9 to 0.11 μm (also, the D_s decreased from 2.9 to 0.17 μm) with increasing the amount of EPR-M to 100 wt% in the rubber phase. This implies that with increasing the amount of EPR-M, the amount of in situ graft copolymer formed from the reaction between the amine and the anhydride groups was increased. Also, the interface between AN and EPR phases was gradually rougher as the content of EPR-M increased. This suggests that EPR-M played a role in an effective compatibilizer of AN/EPR blend since the reaction between the maleic anhydride in EPR-M and the amine group in AN occurs easily at higher temperature [18–23].

Fig. 3 shows plots of η^*, G' and G'' with ω for AN–EPR-M(x) as well as neat AN, EPR, and EPR-M. The η^* of neat EPR is very similar to that of neat AN at lower ω, whereas the η^* of neat EPR is smaller than that of neat AN at higher ω. The η^* of AN–EPR-M(0) becomes lower than that of a blend component (neat AN and EPR), while shear thinning becomes more severe compared with blend components. This is often observed for an immiscible blend when the dispersed domains are easily deformed along the flow direction [25]. Neat AN had the lowest G' among all materials employed in this study. With increasing the amount of EPR-M, η^*, G' and G'' of AN–EPR-M(x) increased due to the increased amount of graft copolymers formed at the interface [19–24]. At lower ω, the increase in G' with the amount of EPR-M was much larger compared with η^* and G'', since G' is more sensitive to the amount of graft copolymers. When the added amount of EPR-M was 100 wt%, a yield behavior at lower frequencies was observed, as shown in Fig. 3(b).

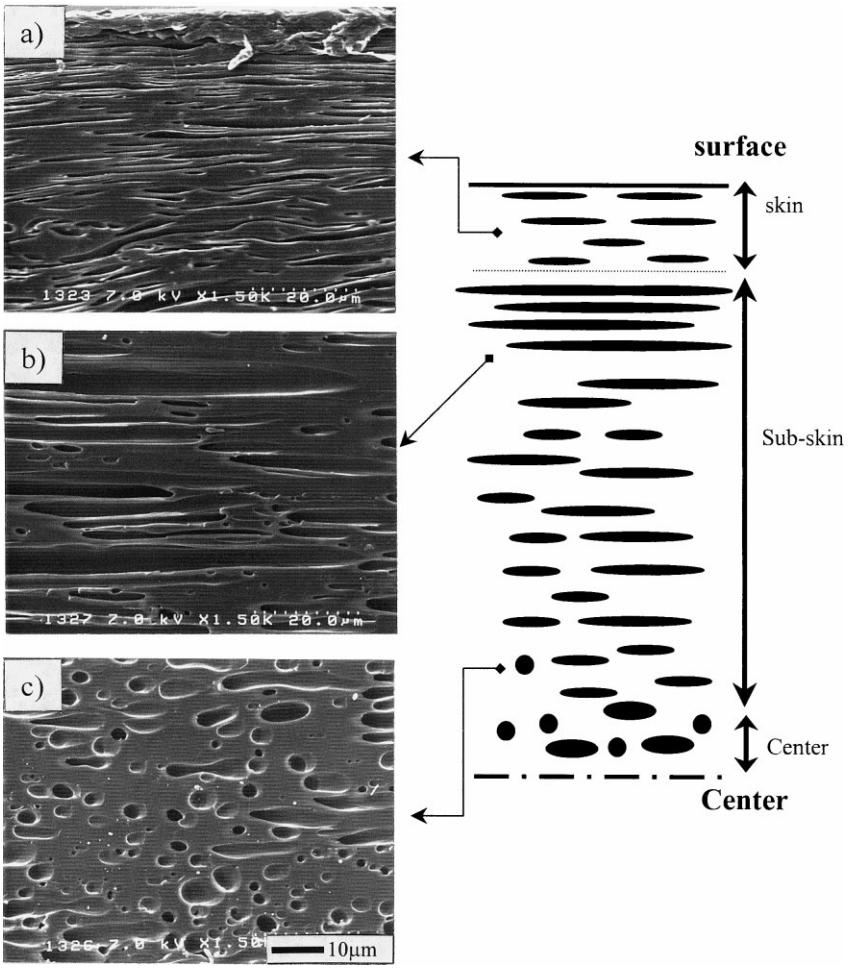

Fig. 4. SEM images (*xy*-plane) of AN–EPR-M(0) without weld-line at three different positions across the thickness: (a) skin layer; (b) sub-skin layer; and (c) near center. The schematic of the morphology is shown in the right panel.

3.2. Morphology of the injection molded blend

Figs. 4–7 give SEM micrographs at three different positions across the thickness of specimens for AN–EPR-M (x; $x = 0; 6; 20; 100$) without a weld-line. Typical skin, sub-skin, and core morphologies were seen for all specimens. But, for AN–EPR-M(0) blend, most of the dispersed domains even at the center regions are also elongated; thus, a core region is not clearly separated from the sub-skin layer. The sub-skin layer in this blend covers almost (more than 90%) the entire thickness. The formation of skin–core morphologies can be explained as follows. Near the cavity wall, the molten polymers are immediately solidified; thus the "skin" layer was formed, implying that the dispersed domains near the wall are not much elongated by the shear stress. The largest elongation of dispersed domains toward the flow direction was found at the "sub-skin" layer, where the shear stress is the largest. Near the center (or the "core" region) where the stress was the lowest, the dispersed domain structures are not changed with the flow; thus, spherical domains are observed [10,12].

It is seen in Figs. 4–7 that increasing the amount of EPR-M significantly decreased the thickness of the sub-skin layer. Schematics of morphologies for AN–EPR-M(0) and AN–EPR-M(100) are added in the right panel of Figs. 4 and 7, respectively. When the EPR-M content increased to 6 wt%, the sub-skin layer thickness reduced to one-third (~1000 μm). For AN–EPR-M(100), the thickness of the sub-skin layer was very much reduced (about 2% of the thickness). The decrease in skin (or subskin) layer with increasing amount of EPR-M is consistent with the results for a blend of PA6/HDPE with an ionomer [11]. However, in Ref. [11] the sub-skin region for this blend without the compatibilizer consists of only 30% of the whole thickness, which is quite small compared with our blend system where this region covers almost the entire thickness. Furthermore, the sub-skin layer for PA6/HDPE blend with a compatibilizer is still large (14% of whole thickness). The different behaviors between HDPE/PA6 and our blend system might be due to the semi-crystalline nature of PA6 compared with amorphous AN, different compatibilization methods (physical versus chemical compatibilizations) and viscosity ratio between the matrix and the dispersed phase.

Also, the degree of elongation (L/D) of the dispersed

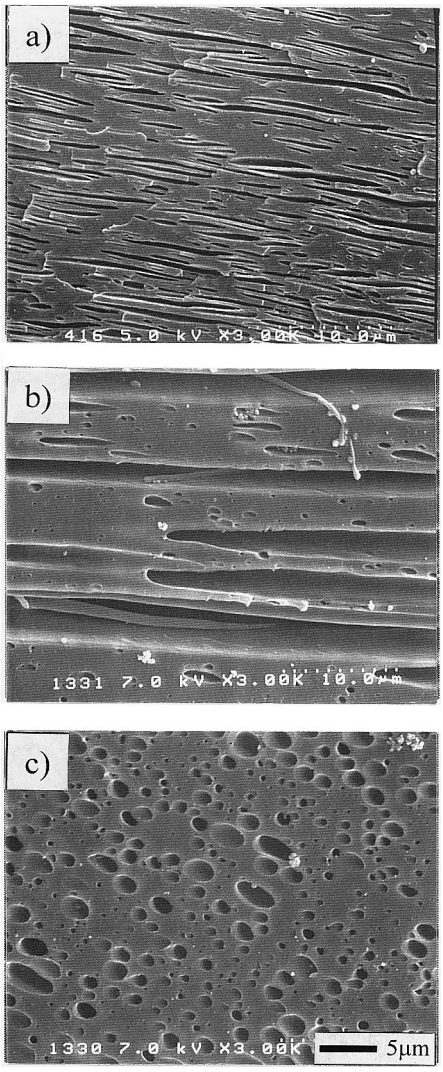

Fig. 5. SEM images (*xy*-plane) of AN–EPR-M(6) without weld-line at three different positions across the thickness: (a) skin layer; (b) sub-skin layer; and (c) core.

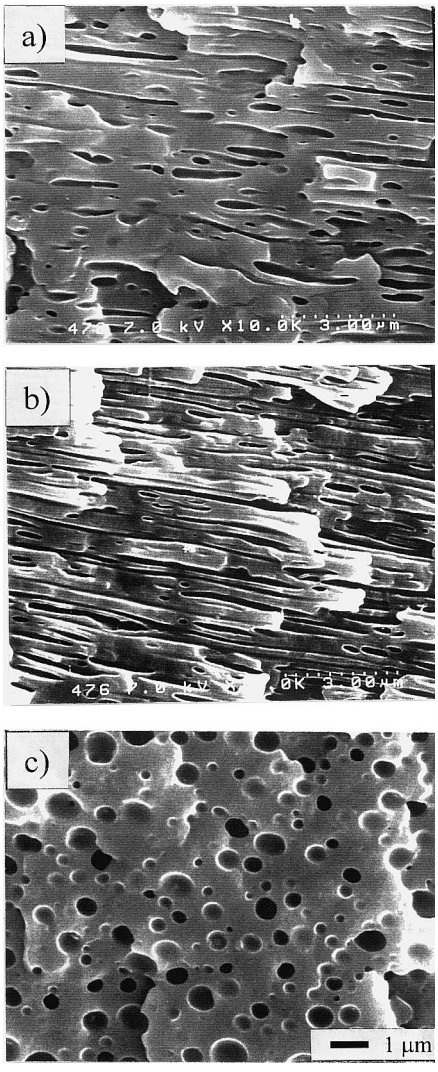

Fig. 6. SEM images (*xy*-plane) of AN–EPR-M(20) without weld-line at three different positions across the thickness: (a) skin layer; (b) sub-skin layer; and (c) core.

domains as well as the dispersed-domain size decreased with increasing the amount of EPR-M, as shown in Table 1. Furthermore, the separation of the skin layer from the sub-skin layer was not distinct with increasing the amount of EPR-M. The skin layer was very small for AN–EPR-M(100). The value of D_n at the core (or center) region is similar to that of the extruded pellet. Also, the difference in D_s between these two decreased with increasing the amount of EPR-M due to reduced coalescence of dispersed domains.

Fig. 8 gives the SEM image at three different positions across the thickness of the weld-line specimen for AN–EPR-M(0) near the weld-line. The schematic of this morphology is shown in the right panel in Fig. 8. Similar SEM images are shown in Figs. 9 and 10 for AN–EPR-M(20) and AN–EPR-M(100), respectively. All blends with weld-lines have a V-notch at the weld line where two fronts meet each other. Furthermore, the shape of the weld-line as shown in the dotted line is not straight but exhibits an oxbow type, which is consistent with the result reported by Jarus et al. [18]. We classify three regions (I), (II), and (III) for weld-line specimens: region (I) near the V-notch; region (II) corresponding to the sub-skin layer for a non-weld specimen; and Region (III) near the center. It is seen in Fig. 8 for AN–EPR-M(0) that the dispersed domains are aligned toward the thickness direction at Region (II). Even near the center, dispersed domains are aligned toward the thickness direction. The largest elongation of dispersed domains in non-weld specimens toward the flow direction occurs at Region (II). Thus, the elongation of dispersed domains toward the thickness direction near the weld-line for weld specimens would be largest at this region because of the biaxial stretching of dispersed domains induced by fountain flow. However, the domains are aligned toward the flow direction far away from the weld-line where the morphologies are essentially the same as those for non-weld specimens.

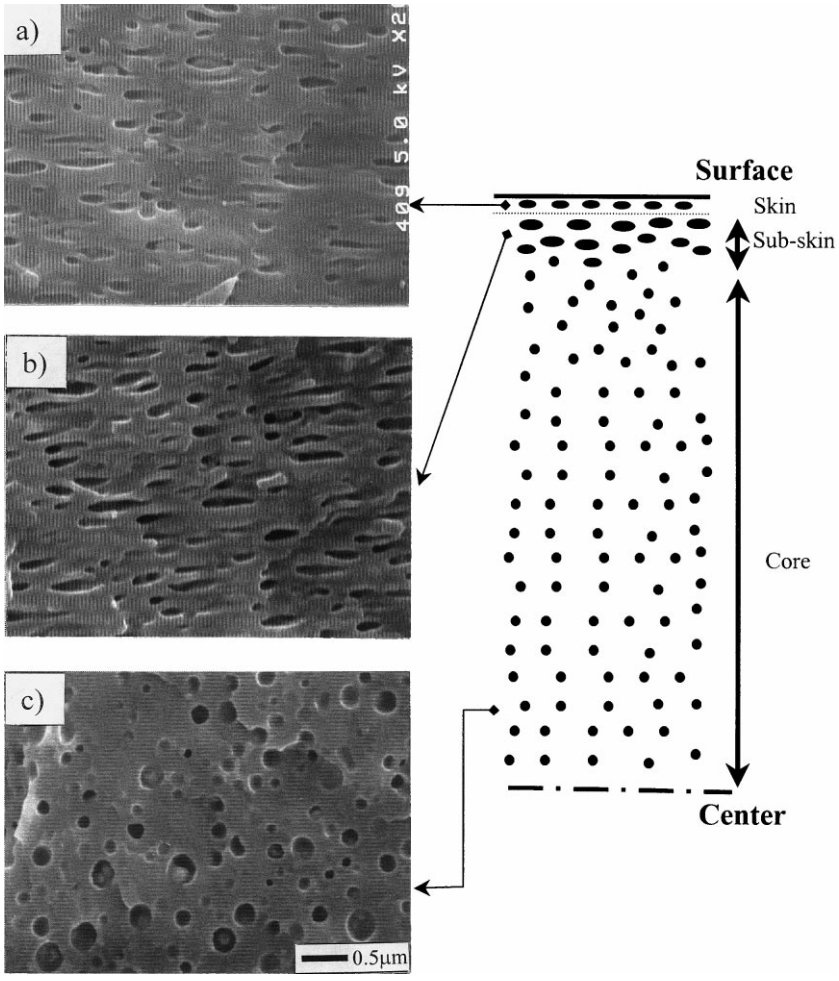

Fig. 7. SEM images (*xy*-plane) of AN–EPR-M(100) without weld-line at three different positions across the thickness: (a) skin layer; (b) sub-skin layer; and (c) core. The schematic of the morphology is shown in the right panel.

Near the center position of the thickness, we observed that the dispersed domain size with spherical shapes inside the weld-line zone is smaller than that outside the weld-line zone. Also, the elongation of smaller domains is barely observed. These smaller domains are formed by the breakup of highly elongated dispersed domains during the cooling process. However, near the surface, these domains do not have enough time to relax due to faster cooling; thus those are not broken into smaller domains with spherical shapes. These smaller domains are not observed for AN–EPR-M(20) and AN–EPR-M(100) where the degree of elongation of dispersed domains toward the thickness direction is much smaller than that for AN–EPR-M(0), although some domains are elongated at Region (II). Furthermore, the contact width, or weld-line width along the sample length direction, defined as the region where the dispersed domains at Region (II) are elongated toward the thickness direction, was the largest (~500 μm) for AN–EPR-M(0). With increasing EPR-M content, this width decreases (~300 μm for AN–EPR-M(6) and less than 50 μm for AN–EPR-M(100)). Also, the height of this region decreases with increasing EPR-M content. For instance, this height for AN–EPR-M(0) covers almost all of the thickness, whereas for AN–EPR-M(100) it is reduced to ~5% of the entire thickness.

3.3. Tensile and impact properties

Fig. 11 gives plots of tensile stress (σ) versus tensile strain (ϵ) as functions of the amount of EPR-M for specimens with and without weld-lines. The values of tensile properties of all blends and neat AN with and without weld-lines are listed in Table 2. Also, the Izod IS of all specimens is added to Table 2. The elongation at the break (ϵ_b) and the stress at the break (σ_b) of neat AN without weld-line are 123.0% and 65.3 MPa, while those for a neat AN with weld-line are 103.4% and 63.5 MPa. Also, both specimens showed yielding behavior. Thus, ϵ_b and σ_b of a neat AN with weld-line do not decrease much compared with those without weld-lines, even though AN is an amorphous polymer. It is reported that for an amorphous material such as PS and PMMA, the ϵ_b of specimens with weld-line was about one-half to one-third that without weld-lines [3,8]. The small decrease in ϵ_b for neat AN with

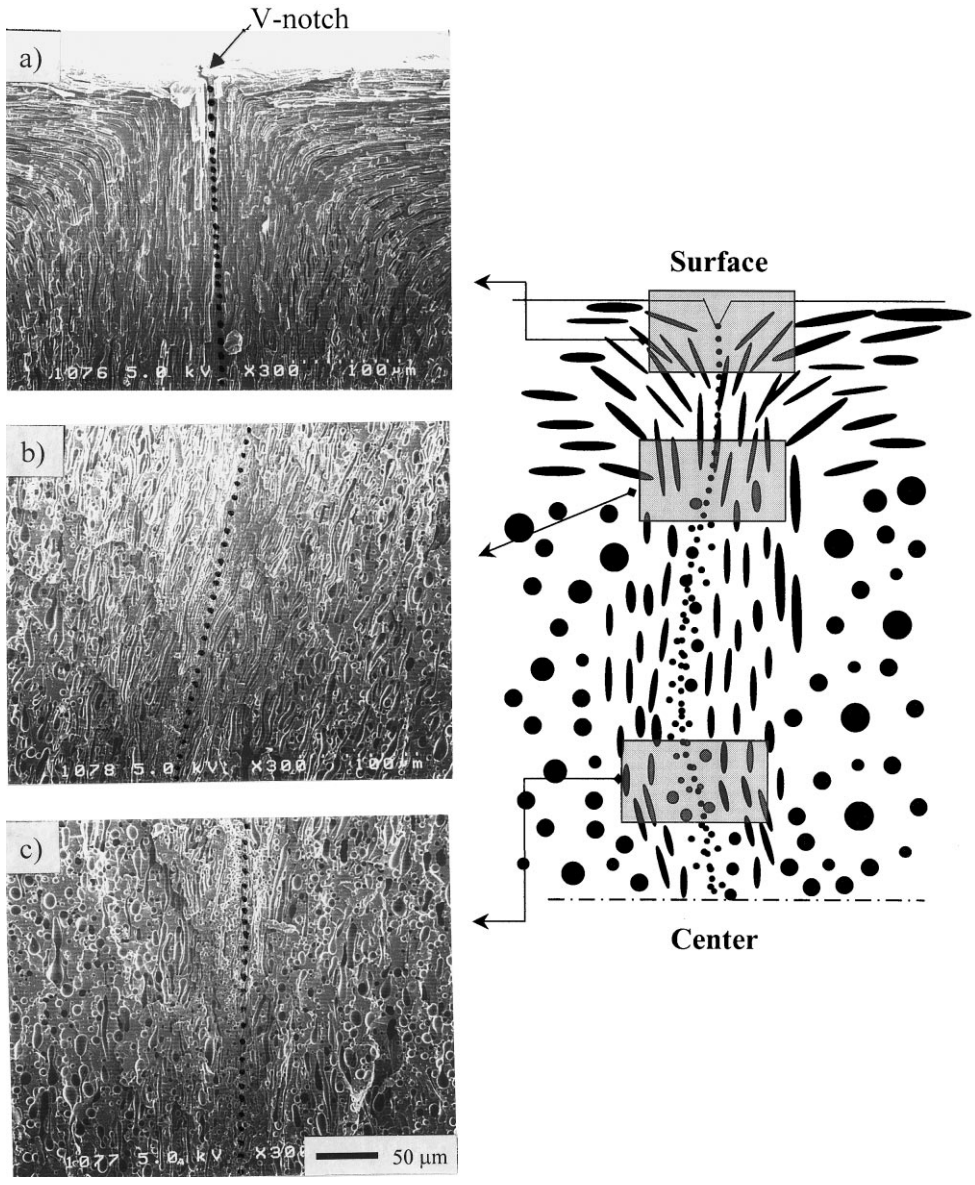

Fig. 8. SEM images (*xy*-plane) of AN–EPR-M(0) with weld-line at three different positions across the thickness: (a) Region (I); (b) Region (II); and (c) Region (III). The schematic of the morphology is shown in the right panel. Weld-line across the thickness is given in dotted line.

weld-lines compared to a non-weld specimen is due to the ductile behavior of AN; thus the tensile speed of 5 mm/min is not enough to give a significant change in ϵ_b of specimens depending upon the weld-line. However, as shown in Table 2, the IS of a neat AN with weld-lines is 14.5 J/m, which is just half of that (31.5 J/m) of a non-weld specimen, which clearly demonstrates the effect of the weld-line.

But the values of ϵ_b for AN–EPR-M(6) and AN–EPR-M(20) with weld lines are much smaller (at least one order of the magnitude) than those without weld-lines as shown in Table 2. This might be due to the difference in the orientation of the dispersed domains; the dispersed domains at the sub-skin layer for non-weld specimens are aligned parallel to the tensile force direction, while those at the sub-skin layer for weld specimens are aligned perpendicularly to the tensile force direction. The degree of orientation of the dispersed domains for AN–EPR-M(100) was sharply decreased compared with that for AN–EPR-M(20) (see Figs. 6 and 7). It is known that a specimen with dispersed domains aligned along the tensile direction has larger ϵ_b than another with dispersed domains aligned perpendicularly to the tensile direction, as long as the interfacial adhesion strength between the phases is good enough. The effect of the V-shape notch found in weld specimens on the tensile strain and strength cannot be excluded [8]. In order to study this effect, we carefully removed the V-notch by polishing the specimen. We found that the increment of ϵ_b for a specimen after the V-notch was removed was negligible. For instance, ϵ_b for a AN–EPR-M(20) after the V-notch was removed was 4.3%, which is within the experimental error

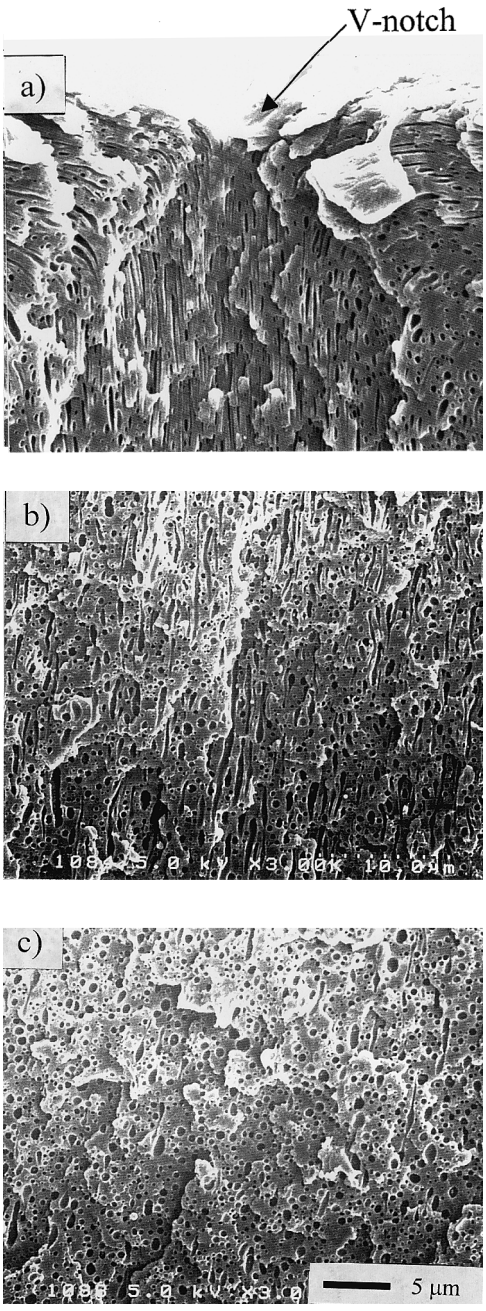

Fig. 9. SEM images (*xy*-plane) of AN–EPR-M(20) with weld-line at three different positions across the thickness: (a) Region (I); (b) Region (II); and (c) Region (III).

of that with the V-notch. We found that the existence of V-notch does not change other tensile properties.

With increasing the amount of EPR-M, the value of ϵ_b for specimens without weld-lines increased from 7.7 to 140.5%, whereas that for specimens with weld-lines increased from 1.8 to 33.0%. We found that the fracture of all specimens with a weld-line was initiated at the weld-line. Also, except for AN–EPR-M(100), all blends with weld-lines showed brittle fracture mode; thus, there is no yield (for instance, see Fig. 12(a) for AN–EPR-M(0)). But, AN–EPR-M(100) with weld-line showed ductile fractured mode, and necking and yielding were clearly seen, as shown in Fig. 12(b) where the fracture surface with highly yielded zone was observed. But, all blends without weld-line showed necking and yielding, and the degree of necking increased with increased amount of EPR-M. On the basis of the results given in Fig. 11, the values of ϵ_b depending upon EPR-M content are given in Table 2.

Interestingly, a sharp increase in ϵ_b for a non-weld specimen was noticed between AN–EPR-M(6) and AN–EPR-M(20), while that for a weld specimen was noticed between AN–EPR-M(20) and AN–EPR-M(100). It is known that ϵ_b of a blend depends upon the morphology of dispersed domains and the adhesion strength between the matrix and the dispersed domains. For a non-weld specimen, the degree of the elongation of dispersed domains toward the tensile direction for AN–EPR-M(100) is much less than that for AN–EPR-M(20), while the adhesion strength for the former is larger than that for the latter. Thus, ϵ_b of these two blends does not change much, since these two effects are counterbalanced. But for weld-specimens, dispersed domains located at the sub-skin layer for AN–EPR-M(100) are still elongated perpendicularly to the tensile direction. In this situation, since the adhesion strength effect is much more important compared with the domain orientation effect, ϵ_b for AN–EPR-M(100) is much larger than that for AN–EPR-M(20). However, the ϵ_b for AN–EPR-M(100) with weld-line was still small compared with a non-weld specimen. This is due to the morphology difference between a specimen without weld-lines and a specimen with weld-lines.

The behaviors in ϵ_b are consistent with the IS results, as shown in Table 2 (also see Fig. 13). The IS of AN–EPR-M(0) without a weld-line was 69 J/m, which is about three times that (25.6 J/m) of the same blend with a weld-line. Since the IS of neat AN without a weld-line is just twice that of neat AN with a weld-line, the additional decrease in IS for AN–EPR-M(0) with weld-lines is due to the domain alignment toward the thickness direction near the weld-lines, as shown in Fig. 8. Interestingly, the IS of a non-weld specimen of AN–EPR-M(20) is even larger than that of AN–EPR-M(100), while the IS of a weld-line specimen for AN–EPR-M(20) is smaller than that of AN–EPR-M(100). This is consistent with previous reports that non-weld specimens of Nylon 6/EPR blend have the largest IS when the dispersed domain size is 0.2–0.3 μm [22]. If the dispersed domain size is too small (say less than 0.2 μm), the interparticle length becomes too short to resist the fracture.

It is noted that the weld-line strength of an amorphous polymer can be recovered by sufficient annealing [26–28]. Thus, when we compared the IS of weld-line specimens without annealing with that with annealing, the effect of dispersed domain morphology itself on IS can be examined. When a neat AN specimen with weld-lines was annealed at 180°C for 48 h, the IS increased from 15 to 27 J/m, which is ~90% of the IS of a non-weld specimen (IS = 31 J/m). We

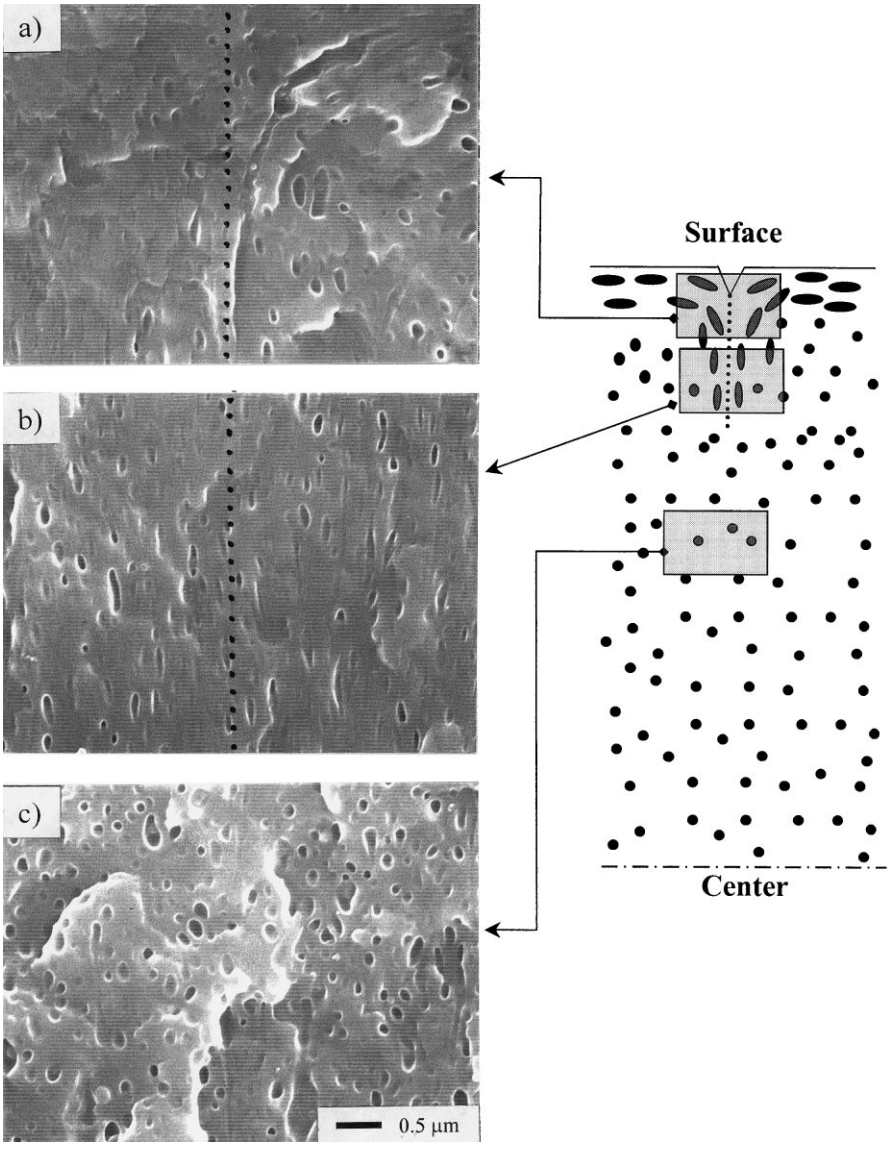

Fig. 10. SEM images (*xy*-plane) of AN–EPR-M(100) with weld-line at three different positions across the thickness: (a) Region (I); (b) Region (II); and (c) Region (III). The schematic of the morphology is shown in the right panel. Weld-line across the thickness is given in dotted line.

found that annealing time of 180°C for 24 h gives essentially the same results for IS. Thus, we considered that the annealing condition employed in this study was sufficient for AN-6 chains near the weld-line to diffuse into much larger length than the radius gyration of AN-6, as corroborated by the calculation of the self-diffusion coefficient (D) of AN at 180°C as follows [29]:

$$D = \frac{G_N^0}{135}\left(\frac{\langle r^2\rangle}{M}\right)\left(\frac{M_e}{M}\right)^2\left(\frac{M}{\eta_0(M_c)}\right) \tag{3}$$

where G_N^0 is the plateau modulus, $\langle r^2\rangle^{1/2}$ is the end to end distance, M_e the entanglement molecular weight, M_c the critical molecular weight for the viscosity, and $\eta_0(M_c)$ the zero-shear viscosity at M_c. Since the values of M_e, M_c, and $\langle r^2\rangle^{1/2}$ for AN are not available in the literature, we assumed these values are similar to those for polyamide 6 ($M_e = 1980$, $M_c = 5020$, and $\langle r^2\rangle/M = 0.00853\ \text{nm}^2/(\text{gr/mol})$ [30]. Also, it was assumed that $G_N^0 = (4/5)\rho RT/M_e$ in which ρ is the density (1.08 g/cm^3 [31]), R the gas constant, and T the absolute temperature. Finally, $\eta_0(M_c)$ is calculated from the measured $\eta_0(M_w)$ of 4.92×10^4 *Pa s* at 180°C:

$$\eta_0(M_c) = \eta_0(M_w)\left(\frac{M_c}{M_w}\right)^{3.4} \tag{4}$$

Substitution of all parameters with $M_w = 47\,000$, we obtain $D = 3.8 \times 10^{-13}$ cm^2/s, which gives the length ($x = 2\sqrt{Dt}$) for AN-6 chain to diffuse at 180°C for 48 h to be 5.1 μm. Even if we consider that some uncertainty is incurred in estimating certain parameters, we conclude that the distance

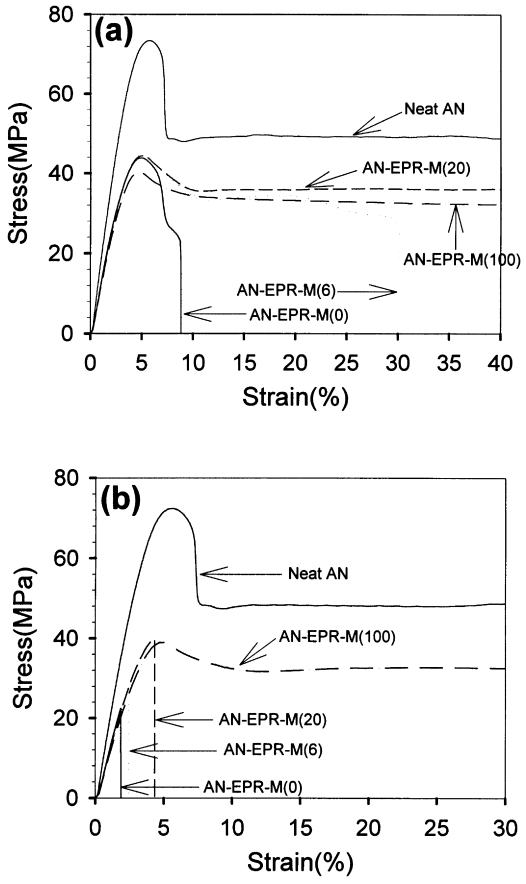

Fig. 11. Stress–strain curves for blends and neat AN: (a) without; and (b) with weld-lines.

for AN-6 chains to diffuse under the above experimental condition is much larger than the radius of gyration (0.008 μm) of AN-6. Thus, the poor adhesion of AN-6 chains themselves near the weld-line is completely recovered by annealing.

We found that the IS of AN–EPR-M(6) after annealing at 180°C for 48 h was just 39 J/m, which is almost the same as that (36 J/m) without annealing. Similar results are found for AN–EPR-M(0). In these two blends, annealing does not affect the IS. Because the dispersed domains are severely elongated toward the direction of the thickness for these two blends, improved mechanical properties upon annealing are not expected even when matrix chains of AN diffuse significantly. Thus, the mechanical properties of a blend with weld-lines depend greatly upon the morphology of dispersed domains. On the other hand, the IS of weld-line specimens of AN–EPR-M(20) and AN–EPR-M(100) annealed at 180°C for 48 h were increased to 187 and 305 J/m, respectively. Thus, in these two blends, annealing enhanced the IS. But the IS of weld-line specimens of AN–EPR-M(20) with annealing is still lower (~one-third) than that of non-weld specimens, whereas the IS of weld-line specimens of AN–EPR-M(100) with annealing approaches (~80%) that of non-weld specimens. This is because the elongated dispersed domains for AN–EPR-M(100) are not distinct compared with AN–EPR-M(20) (compare Fig. 10 with Fig. 9). These results led us to conclude that the IS of weld-line specimens, where there is higher elongated dispersed domain toward the direction of thickness, would not increase significantly even if a long annealing (or healing) is carried out. This is the main difference between weld-line specimens of amorphous homopolymer and those of polymer blends.

The yield stress (σ_y) depends upon the blend morphology and the interfacial adhesion between the two phases. The stronger the interfacial adhesion and the more elongation of dispersed domains toward the tensile direction, the larger the σ_y. With increasing EPR-M, the adhesion increased, whereas the degree of the elongation of dispersed domains decreased. Combining these two conflicting effects, σ_y of specimens without weld-lines would not change much with EPR-M content. At higher EPR-M content, the degree of elongation decreased significantly as shown in Figs. 6 and 7; thus σ_y decreased. The stress at the break (σ_b) increased with increasing EPR-M content up to 20 wt%, irrespective of the existence of the weld-line. Also, σ_b of AN–EPR-M(20) without weld-lines was a little larger than that of AN–EPR-M(100) without weld-lines. This is due to the

Table 2
Tensile properties and Izod impact strength (IS) of blends and neat AN without and with weld-lines

Blend type	E (GPa)	σ_y (MPa)	ϵ_y (%)	σ_b (MPa)	ϵ_b (%)	IS (J/m)
Without weld-line						
Neat AN	2038	73	5.6	65	123	31
AN–EPR-M(0)	1460	44	4.8	20	8	69
AN–EPR-M(6)	1408	45	5.0	25	33	84
AN–EPR-M(20)	1394	44	5.0	50	137	542
AN–EPR-M(100)	1337	40	4.8	46	141	372
With weld-line						
Neat AN	2020	73	5.6	63	103	15
AN–EPR-M(0)	1430	No yielding	No yielding	23	1.8	26
AN–EPR-M(6)	1378	No yielding	No yielding	29	2.4	36
AN–EPR-M(20)	1305	No yielding	No yielding	39	4.4	116
AN–EPR-M(100)	1275	39	4.6	31	33	266

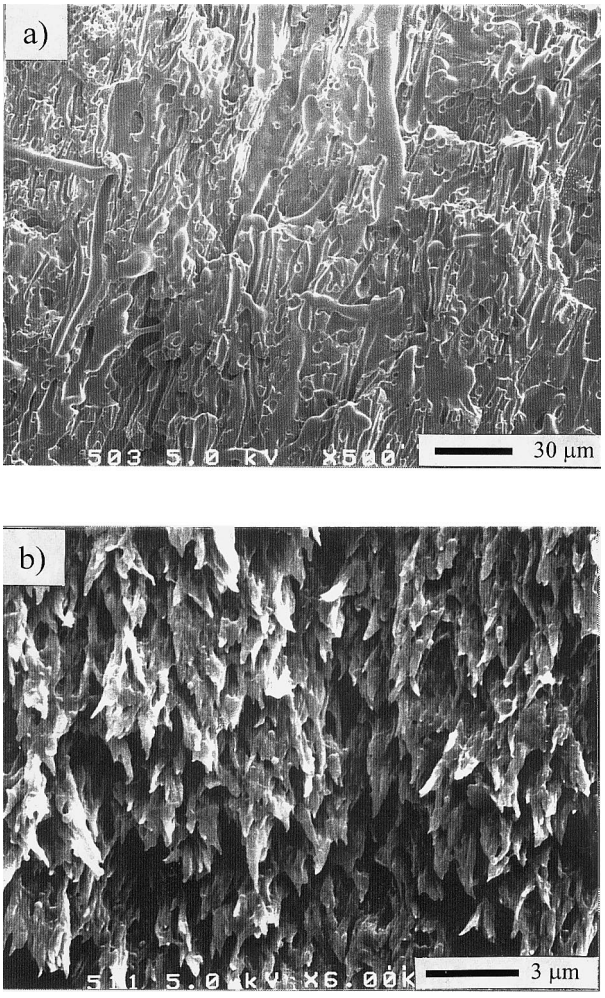

Fig. 12. SEM images of the fracture surface observed at region (II) (corresponding to Fig. 8(b) and Fig. 10(b)) for: (a) AN–EPR-M(0); and (b) AN–EPR-M(100) with weld-lines.

degree of the elongation of the dispersed phase toward the tensile direction for AN–EPE-M(20) without weld-lines, even though the adhesion of the former is larger than that of the latter blend.

Interestingly, σ_b of AN–EPR-M(20) with weld-lines was a little larger than that of AN–EPR-M(100) with weld-line, even though the degree of elongation of the dispersed domains aligned perpendicularly to the tensile direction for the former is larger than that of the latter specimen, and the adhesion of the former is worse than that of the latter. This is due to the different fracture mechanism of the two specimens; AN–EPR-M(20) with weld-lines was fractured before reaching a yield, while AN–EPR-M(100) with weld-lines was fractured after a yield even though ϵ_b was not large. It is usually observed that tensile stress decreases much after a yield point; thus, σ_b of a specimen is lower than σ_y without significant stress hardening. Only for blends (AN–EPR-M(20) and AN–EPR-M(100) without weld-lines) with larger ϵ_b; does σ_b become larger than σ_y. Therefore, it is more reasonable to compare σ_y of a

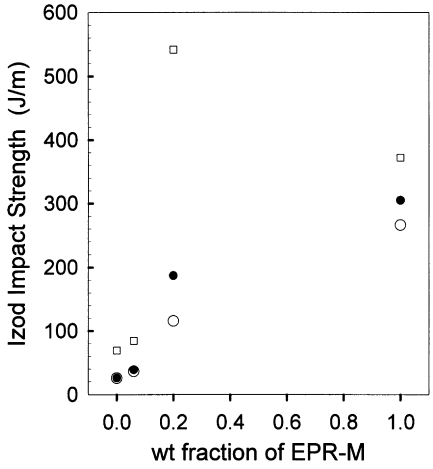

Fig. 13. Izod impact strength (IS) versus EPR-M content for blends without weld line (□). These plots for specimens having weld-line are added without further annealing (○) and annealed at 180°C for 48 h (●).

specimen with a yield to σ_b (not σ_y) of another without yielding. The σ_b of AN–EPR-M(20) with weld-lines is similar to σ_y of AN–EPR-M(100) with weld-lines. Also, although σ_b of AN–EPR-M(0) or AN–EPR-M(20) with weld-lines is slightly larger than σ_b of respective blends without weld-lines, the σ_bs of these two with weld-lines are smaller than the σ_ys without weld-lines. Of course, these two blends with weld-lines were fractured before reaching a yield point.

4. Conclusion

In this study, we investigated the effect of EPR-M as a reactive compatibilizer on the weld-line strength of AN/EPR blend to exclude the effect of crystallization. As the amount of EPR-M increased, the dispersed domains were reduced and flow induced morphology was diminished. From rheological measurements, we found that the elastic property and the viscosity were increased as the content of the EPR-M was increased. We have shown that the injection-molded blend exhibited traditional skin–core morphology, which was strongly affected by the amount of EPR-M. At the weld-line, highly anisotropic morphology was observed for low content of EPR-M, while the blend with 100% of EPR-M showed very fine and isotropic morphology. The orientation and deformation of the dispersed phase was reduced at the weld-line with increasing amount of EPR-M.

As the content of EPR-M increased, the elongation at the break (ϵ_b) was greatly improved for the non-weld-line specimens. But the ϵ_b of weld-line specimens was slightly improved. These results imply that the flow-induced morphology as well as the interfacial adhesion is an important factor affecting the tensile strength of non-weld specimens of the blend. At the weld-line, it is estimated that the elongation at the break was much dependent upon the

morphology of the dispersed phase compared with the interfacial adhesion of the dispersed phase. But, the 'V-shaped notch' did not affect the tensile properties except for a slight increase in the tensile modulus for the specimen without a V-notch.

Finally, we have shown that the impact strength of weld-line specimens with significant elongation of dispersed domains would not be improved by a long annealing. Thus, the mechanical properties of polymer blends are much more dependent upon the morphology of the dispersed domains than the annealing effect. And thus, in order to have good mechanical properties of polymer blend with weld-line, the use of a compatibilizer that results in finer morphology independent of external flow is definitely needed.

Acknowledgements

This work was supported by Korea Research Foundation (1998, 1999) and by POSTECH special fund for Research Instrument (1999).

References

[1] Hobbs SY. Polym Engng Sci 1974;14:621.
[2] Malguarnera SC, Manisali A. Polym Engng Sci 1981;21:586.
[3] Malguarnera SC, Manisali A, Riggs DD. Polym Engng Sci 1981; 21:1149.
[4] Nadkarni VM, Ayodhya SR. Polym Engng Sci 1993;33:358.
[5] Meddad A, Fisa B. Polym Engng Sci 1995;35:893.
[6] Kim SG, Suh NP. Polym Engng Sci 1986;26:1200.
[7] Kim JK, Song JH, Chung ST, Kwon TH. Polym Engng Sci 1997;37: 228.
[8] Cho K, Ahn S, Park J, Park CE, An JH. Polym Engng Sci 1997;37: 1217.
[9] Karger-Kocsis J, Csikai I. Polym Engng Sci 1987;27:241.
[10] Fellahi S, Fisa B, Favis BD. J Appl Polym Sci 1995;57:1319.
[11] Fellahi S, Fisa B, Favis BD. Polymer 1996;37:2615.
[12] Fellahi S, Meddad A, Fisa B, Favis BD. Adv Polym Tech 1995;14: 169.
[13] Brahimi B, Ait-Kadi A, Ajji A. Polym Engng Sci 1994;34:1202.
[14] Meklilef N, Ait-Kadi A, Ajji A. Polymer 1995;36:2033.
[15] Takeda K, Janahashi J, Ishihara O. Seikei-Kakou (Japan) 1994;6:504.
[16] Ramjumar DHS, Bhattacharya B, Vaidya UR. Eur Polym J 1996; 32:999.
[17] Ramjumar DHS, Bhattacharya B, Vaidya UR. Eur Polym J 1997; 33:729.
[18] Jarus D, Summers JW, Hiltner A, Baer E. Polymer 2000;41:3057.
[19] Ellis TS. Macromolecules 1991;24:3845.
[20] Ide F, Hasegawa A. J Appl Polym Sci 1974;118:963.
[21] Campbell JR, Hobbs SY, Shea TJ, Watkins VH. Polym Engng Sci 1990;30:1056.
[22] Oshinski AJ, Keskkula H, Paul DR. Polymer 1992;33:268.
[23] Dedecker K, Groeninckx G. Macromolecules 1999;32:2479.
[24] Koriyama H, Oyama H, Ougizawa T, Inoue T, Weber M, Koch E. Polymer 1999;40:6381.
[25] Han CD. Multiphase flow in polymer processing. New York: Academic Press, 1981.
[26] Malguarnera SC, Riggs DC. Polym Plast Technol Engng 1981;17:198.
[27] Wool RP. Polymer, interfaces: structure and strength. New York: Hanser, 1994.
[28] Jud K, Kausch HH, Williams JG. J Mater Sci 1981;16:204.
[29] Graessley WW. J Polym Sci: Polym Phys Ed 1980;18:27.
[30] Heymans N. Macromolecules 2000;33:4226.
[31] Van Krevelen DW. Properties of polymer. 3rd ed. New York: Elsevier, 1990 (p. 86 and 465).